

[Ag₇(H){E₂P(OR)₂]₆] (E = Se, S): Precursors for the Fabrication of Silver Nanoparticles

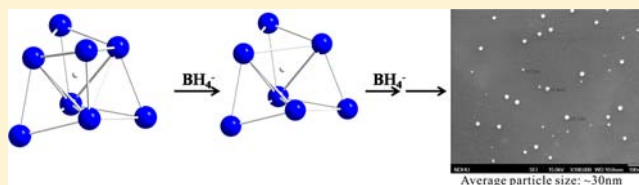
C. W. Liu,^{*,†} Yan-Ru Lin,[†] Ching-Shiang Fang,[†] Camille Latouche,[‡] Samia Kahlal,[‡] and Jean-Yves Saillard^{*,‡}

[†]Department of Chemistry, National Dong Hwa University, Hualien, Taiwan 97401, R.O.C.

[‡]UMR-CNRS, 6226 "Institut des Sciences Chimiques de Rennes", Université de Rennes 1, 35042 Rennes Cedex, France

Supporting Information

ABSTRACT: Reactions of Ag(I) salt, NH₄(E₂P(OR)₂) (R = ⁱPr, Et; E = Se, S), and NaBH₄ in a 7:6:1 ratio in CH₂Cl₂ at room temperature, led to the formation of hydride-centered heptanuclear silver clusters, [Ag₇(H){E₂P(OR)₂]₆] (R = ⁱPr, E = Se (3); R = Et; E = S(4)). The reaction of [Ag₁₀(E){E₂P(OR)₂]₈ with NaBH₄ in CH₂Cl₂ produced [Ag₈(H){E₂P(OR)₂]₆] (PF₆) (R = ⁱPr, E = Se (1); R = Et; E = S(2)), which can be converted to clusters 3 and 4, respectively, via the addition of 1 equiv of borohydride. Intriguingly clusters 1 and 2 can be regenerated via adding 1 equiv of Ag(CH₃CN)₄PF₆ to the solution of compounds 3 and 4, respectively. All complexes have been fully characterized by NMR (¹H, ⁷⁷Se, ¹⁰⁹Ag) spectroscopy, UV–vis, electrospray ionization mass spectrometry (ESI-MS), FT-IR, thermogravimetric analysis (TGA), and elemental analysis, and molecular structures of 3_H and 4_H were clearly established by single crystal X-ray diffraction. Both 3_H and 4_H exhibit a tricapped tetrahedral Ag₇ skeleton, which is inscribed within an E₁₂ icosahedron constituted by six dialkyl dichalcogenophosphate ligands in a tetrametallic-tetraconnective (μ₂, μ₂) bonding mode. Density functional theory (DFT) calculations on the models [Ag₇(H)(E₂PH₂)₆] (E = Se: 3'; E = S: 4') yielded to a tricapped, slightly elongated tetrahedral silver skeleton, and time-dependent DFT (TDDFT) calculations reproduce satisfyingly the UV–vis spectrum with computed transitions at 452 and 423 nm for 3' and 378 nm for 4'. Intriguingly further reactions of [Ag₇(H){E₂P(OR)₂]₆ with 8-fold excess amounts of NaBH₄ produced monodisperse silver nanoparticles with an averaged particle size of 30 nm, which are characterized by scanning electron microscopy (SEM), energy dispersive X-ray (EDX) spectroscopy, X-ray diffraction (XRD), and UV–vis absorption spectrum.



INTRODUCTION

Nanosized, bare metal clusters have broad applications and fundamental importance.¹ However understanding the properties of these nanoparticles has been hindered by the lack of detailed information about how the atoms are actually arranged. Since direct structural information of bare nanoparticles via single crystal X-ray diffraction is not feasible because of the difficulty in crystal growth, the ligand-protected routes do provide an alternative means for diffraction studies from which the exact atomic arrangement can be deduced. This is particularly useful for gold nanoclusters and notable examples are those reported crystal structures of Au₁₀₂(p-SPhCOOH)₄₄,² [Au₂₅(SC₂H₄Ph)₁₈][−],³ [Au₂₅(SC₂H₄Ph)₁₈],⁴ and [Au₃₈(SC₂H₄Ph)₂₄].⁵

Thiolate-protected gold nanoclusters were generally prepared via a simple chemical reduction method, the mixing of gold salts, thiols, and borohydrides.⁶ A legitimate issue is whether hydrides still exist in some of these thiolate-passivated gold nanoclusters or whether gold hydride species are key intermediates en route to the final gold–thiolate nanoclusters. Since hydrido-gold clusters stabilized by sulfur-donor ligands are virtually unknown in the literature,⁷ it will be extremely difficult to address the probable structure relationship between the precursor and its yielded nanocluster. However this is not true for its lighter congener,

silver, owing to the recent structurally characterized silver-only hydrido compounds stabilized by chalcogen-donor ligands such as [Ag₈(H){S₂CC(CN)₂]₆]^{5−},⁸ [Ag₈(H){E₂P(OR)₂]₆]⁺ (E = S, Se),⁹ and [Ag₁₁(H)(S₂CNR₂)₉]⁺.¹⁰ Importantly, two thiolate-protected Ag₇ and Ag₉ clusters, Ag₇(DMSA)₄¹¹ and Ag₉(H₂MSA)₇,¹² where DMSA and MSA represent *meso* 2,3-dimercaptosuccinic acid and mercaptosuccinic acid, respectively, were reported to form via the reaction of silver salt, DMSA in ethanol followed by the addition of NaBH₄ for the Ag₇ nanocluster and the Ag₉ cluster can even be fabricated through a solid state route. Unfortunately the compositions of these subnanoclusters were primarily determined by the electrospray ionization mass spectrometry (ESI-MS) analysis. Thus whether hydrides are present or not in the final silver nanoclusters remains unclear, not to mention their exact atomic arrangements, although some (conflicting) predictions have been made from computational studies.¹³

To explore the structure information of subnanometer-sized silver clusters, we thought it may be possible to structurally characterize some intermediates for which the silver framework may ultimately provide a useful model for the nanocluster

Received: November 14, 2012

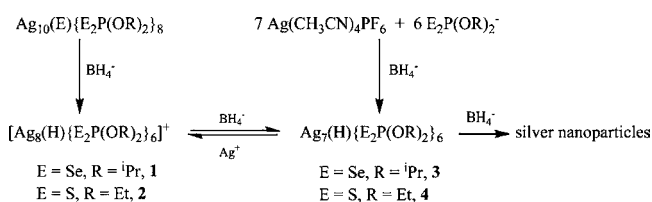
Published: February 5, 2013

formed during the sequential chemical reduction, if less amount of NaBH_4 was added. Thus both clusters $[\text{Ag}_8(\text{H})\{\text{E}_2\text{P}(\text{OR})_2\}_6]^+$ ($\text{E} = \text{Se}, \text{R} = {}^i\text{Pr}, 1$; $\text{S}, \text{R} = \text{Et}, 2$) are utilized to react with borohydrides. Herein the detailed characterizations of two Ag_7HL_6 clusters ($\text{L} = \text{E}_2\text{P}(\text{OR})_2^-$; $\text{Se}, 3$; $\text{S}, 4$) isolated from the reduction of $[\text{Ag}_8\text{HL}_6]^+$ with 1 equiv of BH_4^- are presented. Also reported is the silver nanoparticle synthesis prepared via the chemical reduction route by using the newly isolated Ag_7HL_6 clusters as the precursor.

RESULTS AND DISCUSSION

Preparation, Characterization, and Photophysical Properties of Compounds. Recently we have established that hydride-centered octanuclear silver clusters surrounded by an icosahedral chalcogen cage can be isolated in decent yield from a one-dimensional (1D) pentanuclear extended chain polymer by using the template synthesis method.^{9b} Whereas the hydride provided by BH_4^- acts as the anionic template to yield $[\text{Ag}_8(\text{H})\text{L}_6]^+$, intriguingly the second equivalent of added BH_4^- behaves as a reducing agent to produce $\text{Ag}_7(\text{H})\text{L}_6$ from which a new seven-vertex deltahedron, namely, a tricapped tetrahedron, is demonstrated. The synthesis of $\text{Ag}_7(\text{H})\text{L}_6$ was originally achieved from either the stoichiometric reaction of silver salts, dichalcogenophosphates, and borohydrides or the reaction of $\text{Ag}_{10}(\text{E})\text{L}_8$ with 2 equiv of BH_4^- in $\sim 70\%$ yield.¹⁴ The latter reaction can be monitored by ^{31}P NMR spectroscopy, and it clearly indicates that $[\text{Ag}_8(\text{H})\text{L}_6]^+$ is an intermediate prior to the formation of Ag_7H clusters (Supporting Information, Figure S1a). After rationalization of the cluster transformation, $\text{Ag}_7(\text{H})\text{L}_6$ was formed in decent yield via the reaction of $[\text{Ag}_8(\text{H})\text{L}_6]^+$ with 1 equiv of BH_4^- (Scheme 1). The thus

Scheme 1



obtained new Ag_7 cluster can further react with 1 equiv of silver salt to reproduce the hydride-centered octanuclear silver cluster, $[\text{Ag}_8(\text{H})\text{L}_6]^+$. Indeed the reversible silver uptake and release can also be monitored by ^{31}P NMR spectroscopy (Supporting Information, Figure S1b).

The presence of a hydride within the heptanuclear silver clusters is primarily determined by both ^1H and ^{109}Ag NMR spectroscopy (Figure 1a, b). While the hydride resonance of **3** at 293 K displays an octet peak at 3.50 ppm ($^1J_{\text{H}-\text{Ag}} = 39.4$ Hz), only a broad peak is detected for **4** at ambient temperature. This broad peak cannot be resolved into an octet ($\delta = 5.65$ ppm, $^1J_{\text{H}-\text{Ag}} = 39.6$ Hz) until the temperature was lowered to 223 K. Its integration ratio relative to the methylene protons of the ethyl groups is approximately 1 to 24. The hydride chemical shift is further corroborated by the ^2H NMR spectrum where a broad peak at 3.59 and 6.33 ppm for **3_D** and **4_D**, respectively, was observed at 298 K. Importantly a doublet peak, which arises from the direct coupling to the hydride, appears at 1125.8 ppm ($d, J_{\text{AgH}} = 39.7$ Hz) for **3** and 1116.7 ppm ($d, J_{\text{AgH}} = 41.1$ Hz) for **4** in the ^{109}Ag NMR spectrum. The coupling constant matches well with that identified from the ^1H NMR spectrum. These spectra clearly

indicate that the hydride is coupled to 7 magnetically equivalent silver nuclei, and all 7 silver nuclei are equivalent in the NMR time scale. Moreover, only one chemical shift [83.2 ($J_{\text{PSe}} = 663$ Hz), **3**; 111.8 ppm, **4**] is identified in the VT $^{31}\text{P}\{^1\text{H}\}$ NMR spectrum. A peak at 402 nm and a shoulder at 374 nm are observed for clusters **3** and **4**, respectively, in the UV–vis spectra which can be assigned as a silver to chalcogen charge transfer (MLCT) (vide infra). Besides, both clusters display an orange emission at 77 K ($\lambda_{\text{max}}^{\text{em}} = 626$ and 575 nm) in CHCl_3 glass (Figure 1c). Photophysical data of compounds **3** and **4** are summarized in Table 1.

The heptanuclear silver cluster, **3**, crystallizes in the trigonal space group, $R(-)3$, and its silver framework can be described as a tricapped tetrahedron. The Ag1 and Ag1A atoms located on the crystallographic C_3 axis are each in 50% occupancy. The vertex silver atoms of the inner tetrahedron consist of one Ag1 and three Ag2 atoms, while the Ag3 and their symmetry-equivalent atoms are the three face-capping atoms. The Ag_7 core unit, disordered equally in two orientations, is depicted in Figure 2a along with an interstitial hydride, H0 . The $\text{Ag}_v\text{-Ag}_v$ distances range from 3.169(2) to 3.179(2) Å and those of $\text{Ag}_v\text{-Ag}_{\text{cap}}$ are in the range of 2.942(11)–3.101(14) Å. These distances are comparable with 3.084(2)–3.235(4) ($\text{Ag}_v\text{-Ag}_v$) and 2.989(2)–3.141(2) ($\text{Ag}_v\text{-Ag}_{\text{cap}}$) Å in the hydride-centered octanuclear silver cluster **1**.^{9a} Since the hydride cannot be reliably determined by X-ray diffraction, its relevant metric data are not discussed herein. The Ag_7H core is further inscribed within a distorted icosahedral cage composed of 12 Se atoms of the 6 diselenophosphate ligands (Figure 2b). While the 3 capping silver atoms display an AgSe_3 coordination, it is AgSe_3H identified on the 4 vertex silver atoms. The $\text{Ag}\text{-Se}$ bond lengths are in the range of 2.496(1)–2.902(1) Å and the $\text{Se}\cdots\text{Se}$ bite distances average 3.728(1) Å.

Cluster **4** is iso-structural with **3** (Figure 3a). To the best of our knowledge, these two compounds are the first Ag_7 clusters embedded within an E_{12} ($\text{E} = \text{Se}, \text{S}$) icosahedral cage. The Ag_7 core is also disordered in two parts with the major one in 75% occupancy (Figure 3b). The $\text{Ag}\text{-S}$ distances, of which $\text{Ag}_v\text{-S}$ lengths are longer than $\text{Ag}_{\text{cap}}\text{-S}$ ones, are normal and are in the range of 2.418(3)–2.673(3) Å. The $\text{Ag}\text{-Ag}$ distances are in the range of 2.894(2)–3.153(3) Å. Considering the geometry of the Ag_7 skeleton only, the tricapped tetrahedral core observed in **3** and **4** does occur in one Zintl anion, $[\text{Ag}_7\text{As}_3\text{Te}_{13}]^{4-}$.¹⁵ Selected bond distances and angles of clusters **3** and **4** are listed in Table 2.

The structural relationship between these $[\text{Ag}_7(\text{H})\text{L}_6]$ species and their $[\text{Ag}_8(\text{H})\text{L}_6]^+$ precursors is straightforward. The hydride-centered tricapped tetrahedral core of the former derives formally from the hydride-centered tetracapped tetrahedral (or triakis tetrahedral)¹⁶ core of the latter by simply removing one of its four Ag^+ capping vertices. The vacancies associated with the “missing” capping silver atom in **3** and **4** are located on the top of trigonal faces composed of Ag2A , Ag2E , and Ag2C (Figure 2a) and Ag3C , Ag3D , and Ag4A atoms, respectively (Figure 3b). Removing one capping metal results in the cleavage of three $\text{Ag}\text{-E}$ bonds. This leads to the identification of two kinds of coordination patterns for the dichalcogenophosphate ligands: three in tetraconnective tetrametallic (μ_2, μ_2) and three in triconnective trimetallic (μ_2, μ_1), whereas in the $\text{Ag}_8(\text{H})\text{L}_6$ precursors, all the dichalcogenophosphate ligands have a coordination pattern of (μ_2, μ_2). The molecule itself has an idealized C_3 symmetry. It is of interest to note that the copper framework in $\text{Cu}_7(\mu_4\text{-H})(\text{S}_2\text{CNR}_2)_6$ where the four-coordinate hydride is unequivocally authenticated by neutron diffraction analysis is a tricapped elongated tetrahedron.¹⁷

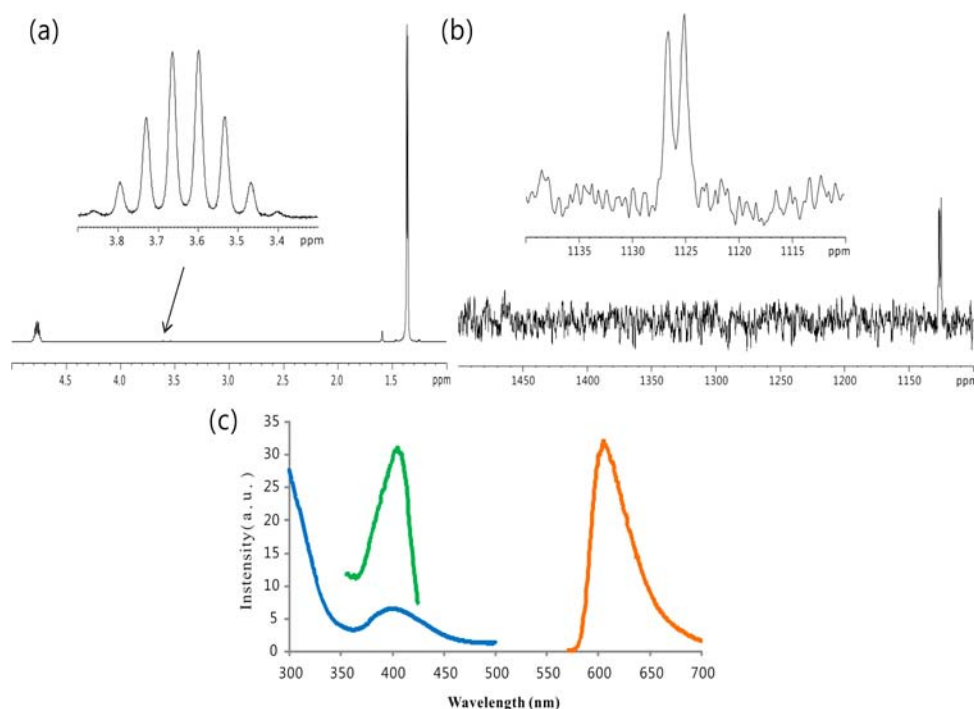


Figure 1. (a) ^1H NMR of **3** with the magnified, hydride resonance shown in the inset. (b) ^{109}Ag NMR spectrum of **3**, (c) Electronic absorption spectrum (blue at 298 K), excitation spectrum (green), and emission spectrum (orange) of **3** at 77 K.

Table 1. Photophysical Data for $[\text{Ag}_7(\mu_4\text{-H})\{\text{E}_2\text{P}(\text{OR})_2\}_6]$ (E = Se, R = ^iPr , **3; E = S, R = Et, **4**)**

compd	state (T/K)	$\lambda_{\text{max}}^{\text{ex}}/\text{nm}$	$\lambda_{\text{max}}^{\text{em}}/\text{nm}$	Stokes shift/ cm^{-1}	$\lambda_{\text{max}}^{\text{ex}}/\text{nm}$ ($\epsilon/\text{dm}^3 \text{ mol}^{-1} \text{ cm}^{-1}$)	lifetime (τ)
3	CHCl_3 , glass(77)	410	626	10135	402 (17,800)	1.0, 7.5 μs
	solid (77)	426	640			
4	CHCl_3 , glass(77)	379	575	8515	374 (21,200)	378, 58 ns
	solid (77)	380	581			

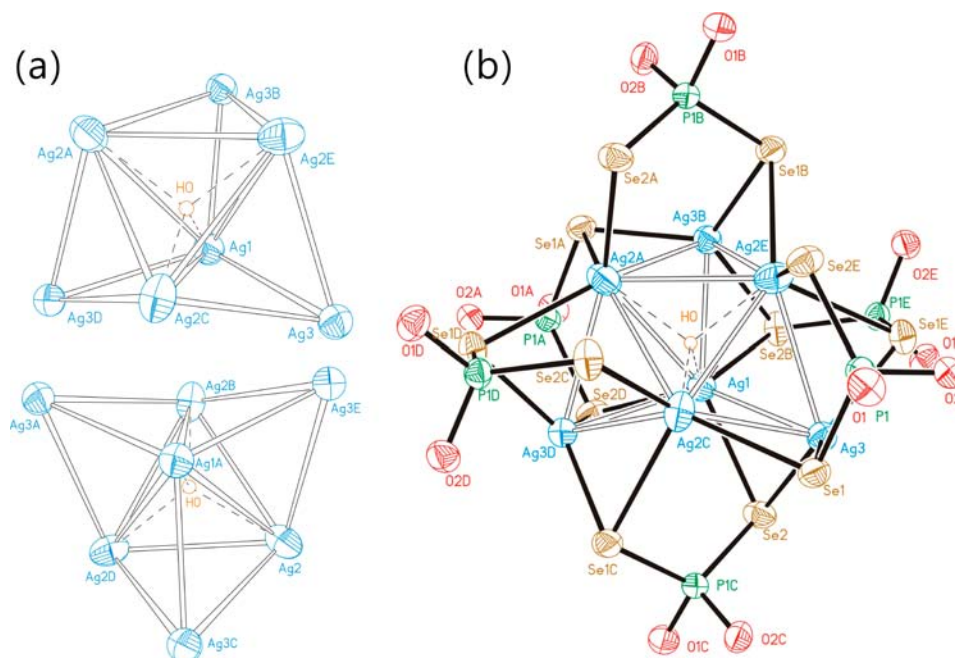


Figure 2. (a) $\text{Ag}_7\text{-H}$ core of **3** disordered in two orientations (50% each). (b) Molecular structure of $[\text{Ag}_7(\mu_4\text{-H})\{\text{Se}_2\text{P}(\text{O}^i\text{Pr})_2\}_6]$ **3** (30% thermal ellipsoid) with isopropyl groups omitted for clarity.

Discrepancies revealed from the results of multinuclear NMR spectroscopy and the single crystal X-ray diffraction need

deliberation. Since two types of connectivities for six $\text{E}_2\text{P}(\text{OR})_2^-$ ligands are observed in both clusters, these should result in two

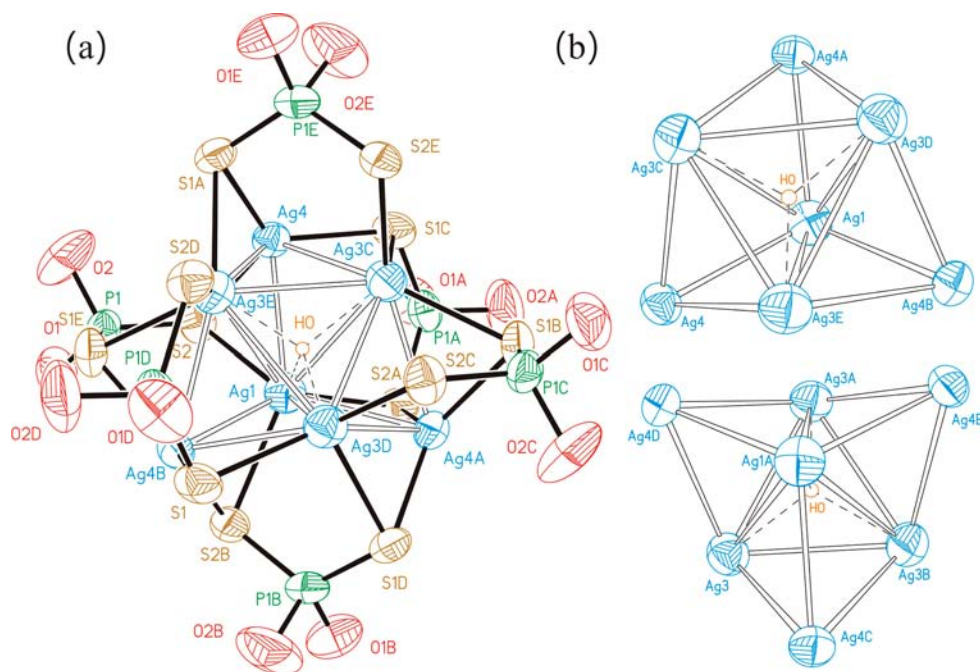


Figure 3. (a) Molecular structure of $[Ag_7(\mu_4-H)\{S_2P(OEt)_2\}_6]$ **4** (30% thermal ellipsoid) with ethyl groups omitted for clarity. (b) The Ag_7H core in **4** disordered in two orientations (top 75%, bottom 25%).

Table 2. Selected Bond Lengths (Å) and Angles (deg) for **3** and **4**^a and for the **3'** and **4'** Optimized Models^b

	3_H	4_H	3'	4'
Ag _v –H	1.785(2), 2.003(2)	1.893(3), 1.942(2)	1.938, 2.005	1.955, 2.001
Ag _v –Ag _v	3.169(2), 3.179(2)	3.149(3), 3.153(3)	3.179, 3.301	3.148, 3.338
Ag _v –Ag _{cap}	2.942(11), 3.050(15), 3.101(14)	2.894(2), 2.910(3), 2.917(3)	3.046, 3.149, 3.218	3.021, 3.120, 3.182
Ag _v –E	2.661(11), 2.733(10), 2.766(12), 2.902(13)	2.626(3), 2.638(3), 2.673(3)	2.728, 2.827, 2.842, 2.899	2.610, 2.715, 2.729, 2.825
Ag _{cap} –E	2.496(10), 2.530(11), 2.611(11)	2.418(3), 2.435(3), 2.457(3)	2.668, 2.696, 2.710	2.565, 2.593, 2.611
E⋯E (bite)	3.728(1)	3.427(4)	3.814, 3.879	3.539, 3.581
E–P	2.151(1), 2.169(2)	1.975(4), 1.979(5)	2.155, 2.219	2.024, 2.035
∠E–P–E	119.28(7)	120.17(16)	121.4	121.9

^aFrom X-ray structures, estimated standard deviations listed in parentheses. ^bFrom DFT geometry optimization.

distinct ³¹P chemical shifts. That only a C₃ rotational axis is present makes the vertex and capping silver atoms non-equivalent. However these are not exactly what we have observed from both VT ³¹P and ¹⁰⁹Ag NMR spectroscopic studies. Thus, fast interchanges between vertex and capping silver atoms must occur in solution, and the exchange rate is so fast that all Ag and P atoms are equivalent on the NMR time scale. It could be due to the asymmetric stretching of Ag–Se(S) bonds driven by the four Ag–H covalent interactions (vide infra) as those proposed for $[Ag_8(H)(i-MNT)_6]^{5-8}$.

Electronic Structure of the Title Compounds. DFT calculations (see Computational Details) on the models $[Ag_7(H)(E_2PH_2)_6]$ (E = Se: **3'**; E = S: **4'**) yielded to a similar optimized tricapped tetrahedral geometry, of C₃ symmetry and characterized as a minimum, whatever the choice was of the starting geometry. Both optimized geometries are in agreement with the X-ray structures (see Table 2). The major difference with the X-ray structures comes from the fact that the (tricapped) central (Ag_v)₄ tetrahedron is more elongated, as exemplified by the corresponding elongated edges which are 3.301 Å (**3'**) and 3.338 Å (**4'**), vs 3.179 Å (**3_H**) and 3.153 Å (**4_H**) (see Table 2). The hydride sits at the center of the tricapped tetrahedron, with Ag–H distances of 2.01 Å (×3) and 1.94 Å (**3'**) and 2.00 Å (×3) and 1.96 Å (**4'**). The natural orbital population analysis leads to

hydride net charges of –0.65 (**3'**) and –0.66 (**4'**). These values are consistent with significant covalent interactions, as found in related species.^{9a,10,17} The ¹H NMR chemical shift of the hydride is computed to be 6.15 ppm for **4'**, in relatively good agreement with the corresponding experimental value of **4_H** (5.65 ppm). As usually observed in the diselenophosphate derivatives, a larger discrepancy is found between the computed hydride chemical shift of **3'** (5.08 ppm) and the experimental value recorded for **3_H** (3.50 ppm). The use of hybrid functionals barely improves the computed chemical shifts (Supporting Information, Table S4). Removing the encapsulated hydride from the $[Ag_7(H)(E_2PH_2)_6]$ gives rise to an empty $[Ag_7(E_2PH_2)_6]^+$ hypothetical species, the equilibrium structure of which is no longer a tricapped tetrahedron but rather resembles a cube having an unoccupied vertex. A similar structure relaxation was computed when removing the hydride from the corresponding $[Cu_7(H)-(S_2CNH_2)_6]$ cluster.¹⁷ The bonding energy between the encapsulated hydride and the unrelaxed $[Ag_7(E_2PH_2)_6]^+$ fragment is equal to 8.54 eV (**3'**) and 8.67 eV (**4'**), whereas the energy lost by the empty $[Ag_7(E_2PH_2)_6]^+$ fragment when distorted from its equilibrium geometry to that it adopts in $[Ag_7(H)(E_2PH_2)_6]$ is 0.73 eV (**3'**) and 0.77 eV (**4'**). These values are consistent with those obtained for the related $[Cu_7(H)-(S_2CNH_2)_6]$ species.¹⁷

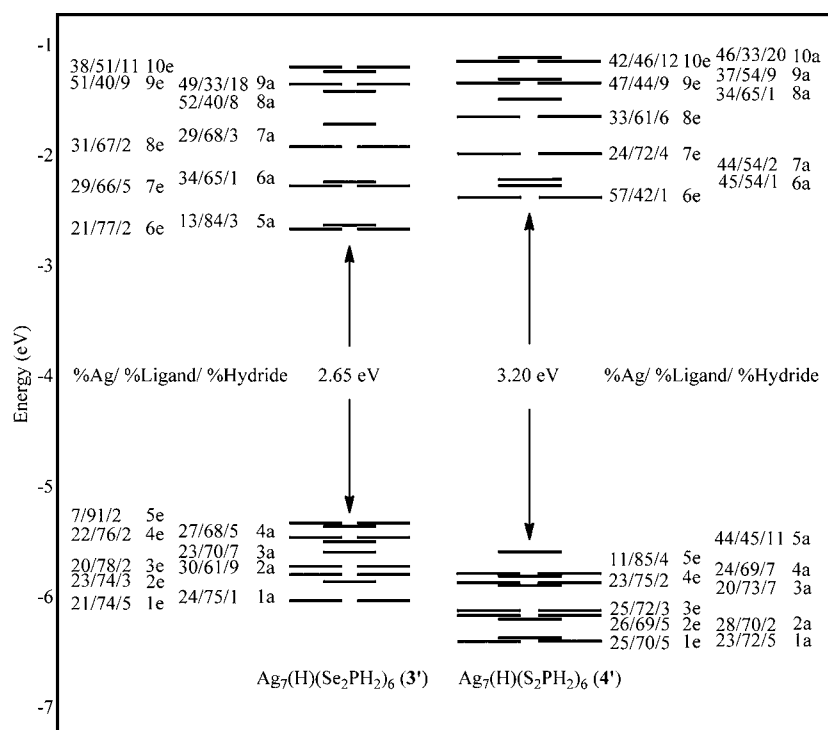


Figure 4. Frontier MO diagrams of 3' and 4' from BP86/LANL2DZ+pol calculations. The numerical values indicate the MO localization (%) in the following order: metals/ligands/ μ_4 -H.

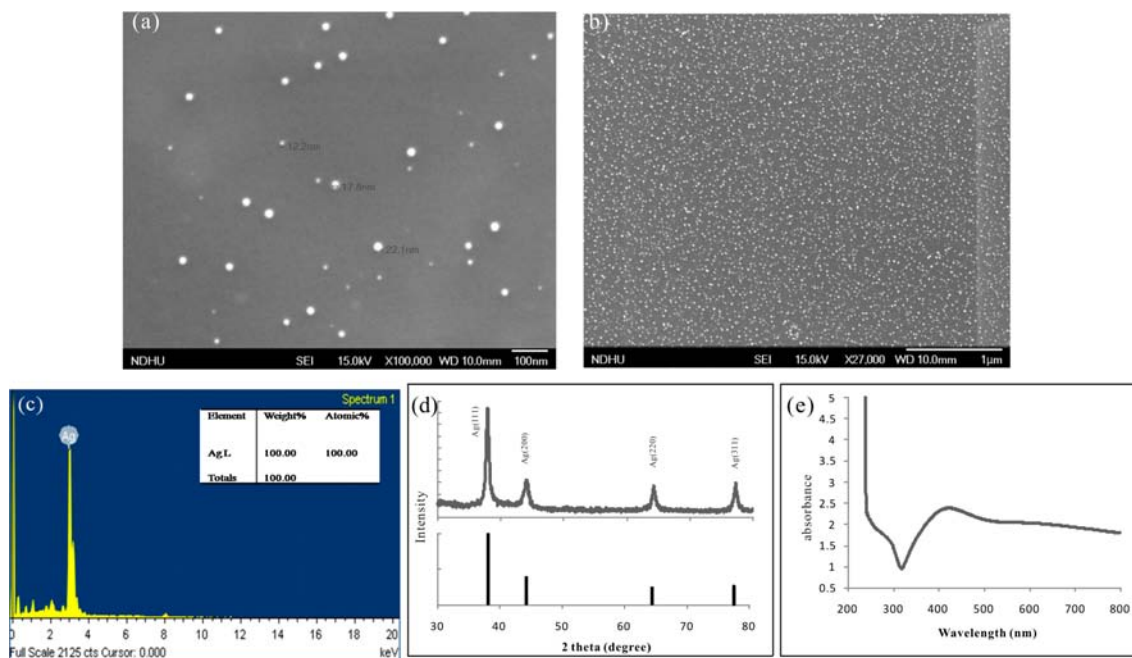


Figure 5. (a) SEM images of the small size Ag nanoparticles. (b) SEM images of the monodisperse Ag nanoparticles. (c) EDX spectrum of Ag nanoparticles. (d) XRD patterns of Ag nanoparticles (top), standard data for Ag JCPDS No. 04-0783 (bottom). (e) The UV-vis spectrum of Ag nanoparticles.

The MO diagrams of 3' and 4' are shown in Figure 4, with the MO localizations listed. Most of the highest occupied and lowest unoccupied orbitals are of dominant ligand (mainly Se/S lone pairs) character, with significant Ag admixture (mainly 4d for the occupied orbitals and 5s/4p for the vacant ones). The small hydride participation to the frontier orbitals of symmetry *a* is consistent with significant covalent interactions with the hosting silver cage. The TDDFT calculations (see Computational

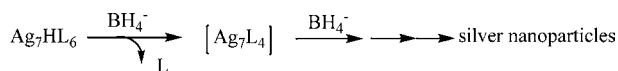
Details) reproduce satisfyingly the UV-vis spectrum with computed transitions at 452 nm (HOMO-2 \rightarrow LUMO+2) and 423 nm (HOMO-6 \rightarrow LUMO) for 3', and 378 nm (HOMO \rightarrow LUMO) for 4'. These transitions are best described as of MLCT type in the case of 3', although mainly 4d(Ag) \rightarrow 5s/5p(Ag) in the case of 4'.

Fabrication of Silver Nanoparticles. Further reaction of Ag₇H clusters with 8-fold excessive amounts of borohydride in

methanol yields silver nanoparticles. The monodisperse silver nanoparticles (Figure 5b) having the average particle size of ~30 nm were fully characterized by scanning electron microscopy (SEM), X-ray diffraction (XRD), energy dispersive X-ray (EDX) spectroscopy, and UV–vis absorption spectrum (Figure 5). The as-synthesized silver nanoparticles, whose purity was confirmed by EDX (Figure 5c), have the fcc structure which is reflected from the XRD and matched with the standard XRD pattern (JCPDS No. 04-0783) (Figure 5d). A typical absorption band arising from the surface plasmon resonance is observed around ~410 nm (Figure 5e),¹⁸ which is in agreement with the average silver nanoparticle size of ~30 nm (Figure 5a).¹⁹

How do these results relate to the growth of silver nanoparticles which are fabricated via a chemical reduction process? Since the ³¹P NMR spectrum of the filtrates suggested the presence of free dtp (L) ligands, thus it is likely that borohydride reduction of the cluster, **4**, leads to the recently reported thiolate-stabilized subnanometer clusters such as Ag₇L₄ containing Ag–Ag bonds,¹¹ which unfortunately has not been isolated in our system. Presumably further rapid reductions of the silver subnanometer clusters yield the Ag(0) nanoparticles. Thus the growth of silver nuclei into nanoparticles is too fast to control the cluster growth kinetics. It is of interest to know that Ag(0) was also produced upon the fabrication of Ag₇(DMSA)₄¹¹ and Ag₉(H₂MSA)₇.¹² Thus the hydrido silver clusters reported herein could be valuable precursors en route to the final silver nanoparticles probably via the formation of transient dithiolate-protected silver subnanoclusters, Ag₇L₄ (Scheme 2). It will be of great interest to uncover the structural details of the latter in atomic resolution.

Scheme 2



In conclusion, this contribution has successfully demonstrated that novel heptanuclear silver clusters stabilized by 6 dichalcogenophosphate ligands and a central hydride can be prepared by the reduction of precursor compounds, [Ag₈(H)-{E₂P(OⁱPr)₂}]⁺, with borohydrides. The presence of hydride is primarily determined by ¹H (²H) and ¹⁰⁹Ag NMR spectroscopy. A hydride-centered tricapped tetrahedral silver core revealed from the XRD study on both compounds **3** and **4** can also be reproduced by DFT calculations on the models Ag₇(H)-(E₂PH₂)₆. Further reductions of Ag₇HL₆ clusters yield highly monodisperse silver nanoparticles with averaged particle size of 30 nm.

EXPERIMENTAL SECTION

General Procedures and Instrumentations. All the reactions were performed in oven-dried Schlenk glasswares by using standard inert-atmosphere techniques. Solvents were distilled prior to use under an inert atmosphere. NH₄S₂P(OEt)₂ was purchased from Aldrich, and all other chemicals were purchased from commercial sources, and used as received. NH₄Se₂P(OⁱPr)₂ was prepared as described in the literature.²⁰ NMR spectra were recorded on a Bruker Avance DPX300 FT-NMR spectrometer at ambient temperature. Residual solvent protons were used as a reference (ppm, CDCl₃, 7.26). The PhSeSePh and H₃PO₄ (85%) were used as an external reference for the ⁷⁷Se (δ = 454 ppm) and ³¹P (δ = 0 ppm) NMR, respectively. ¹⁰⁹Ag NMR spectra of **3** and **4** were recorded on a Bruker Avance III 600NMR. The elemental analyses were performed using a Perkin-Elmer 2400 CHN analyzer. UV–visible absorption spectra were measured on a Perkin-

Elmer Lambda 750 spectrophotometer using quartz cells with path length of 1 cm recording in the 250–750 nm region. Emission spectra were recorded on a Cary Eclipse B10 fluorescence spectrophotometer. ESI-mass spectra were recorded on a Fison Quattro Bio-Q (Fisons Instruments, VG Biotech, U.K.). Melting points were measured by using a Fargo MP-2D melting point apparatus. SEM spectra were recorded on JEOL JSM-7000F. XRD spectra were recorded on Bruker D8 Advance. All infrared spectra were recorded on a Bruker Optics FTIR TENSOR 27 spectrometer at 20 °C using a KBr plate. The lifetimes were recorded on Fluorescence Spectrometers Edinburgh FLSP920 at 77 K.

[Ag₇(H){Se₂P(OⁱPr)₂}]₆, **3_H. *Method A.* To a solution of NH₄[Se₂P(OⁱPr)₂] (0.20 g, 0.615 mmol) and [Ag(CH₃CN)₄]PF₆ (0.297 g, 0.718 mmol) in 20 mL of dichloromethane were added NaBH₄ (0.0039 g, 0.103 mmol), and the mixture was stirred at room temperature for 2 h under nitrogen. The slight yellow solution obtained was filtered and dried in a vacuum. The residue was washed with deionized water and dried under a vacuum to obtain [Ag₇(H){Se₂P(OⁱPr)₂}]₆ as a yellow powder. Yield: 0.234 g (73%). Mp: 150 °C (dec). Anal. calcd for C₃₆H₈₅Ag₇O₁₂P₆Se₁₂: C, 16.64; H, 3.30. Found: C, 17.01; H, 3.24%. ¹H NMR (300 MHz, CDCl₃): 1.36 (d, ³J_{HH} = 3.0 Hz, 72H, CH₃), 3.52 (octet, 1H, μ-H, J_{HAg} = 39.4 Hz, 298 K), 4.76 (m, 12H, CH), ³¹P NMR (121.49 MHz, CDCl₃): 83.2 (J_{P-Se} = 663 Hz). ⁷⁷Se NMR (57.24 MHz, CDCl₃): 2.5 (d, J_{PSe} = 662 Hz). ¹⁰⁹Ag NMR (27.9 MHz, CDCl₃): 1125.8 (d, J_{AgH} = 39.7 Hz). UV–vis [λ_{max} in nm, (ε in M⁻¹ cm⁻¹)], 402 (19,800). ESI-MS (m/z) [M+Ag]⁺ (Cal.): 2705.10 (2706.36). IR, cm⁻¹: 2977.2(m), 965.7(s), 840.2(s), 738.5(m), 535.1(m).**

Method B. The reaction of [Ag₈(H){Se₂P(OⁱPr)₂}]⁺ (0.347 g, 0.122 mmol) with BH₄⁻ (0.0016 g, 0.061 mmol) in 20 mL of chloroform was stirred at room temperature for 3 h under nitrogen. It was washed with deionized water followed by dichloromethane and dried under vacuum to obtain [Ag₇(H){Se₂P(OⁱPr)₂}]₆, **3_H**, as a yellow powder. Yield: 84%.

[Ag₇(D){Se₂P(OⁱPr)₂}]₆, **3_D. It can be synthesized via a similar procedure as described for **3_H**, using NaBD₄ instead of NaBH₄. Yield: 0.255 g (72%). Mp: 142 °C (dec). Anal. calcd for C₃₆H₈₄DAg₇O₁₂P₆Se₁₂: C, 16.63; H, 3.33. Found: C, 16.43; H, 3.76. ¹H NMR (300 MHz, CDCl₃): 1.38 (d, ³J_{HH} = 3.0 Hz, 72H, CH₃), 4.85 (m, 12H, CH), ²H NMR (46.1 MHz, CHCl₃): 3.59 (bs, 1D, 298 K), ³¹P NMR (121.49 MHz, CDCl₃): 83.15 (J_{P-Se} = 662 Hz). ⁷⁷Se NMR (57.24 MHz, CDCl₃): 2.5 (d, J_{SeP} = 651 Hz).**

[Ag₇(H){S₂P(OEt)₂}]₆, **4_H. It was synthesized in a similar manner as described for compound **3_H**. However, NH₄[S₂P(OEt)₂] was used instead of NH₄[Se₂P(OⁱPr)₂]. Yield: 0.302 g (73%). Mp: 128 °C (dec). Anal. calcd for C₂₄H₆₁Ag₇O₁₂P₆S₁₂: C, 15.44; H, 3.29. Found: C, 15.27; H, 3.45%. ¹H NMR (300 MHz, CDCl₃): 1.34 (t, ³J_{HH} = 6.9 Hz, 36H, CH₃), 4.15 (m, 24H, CH₂), 5.65 (octet, 1H, J_{HAg} = 39.6 Hz, 223 K), ³¹P NMR (121.49 MHz, CDCl₃): 111.8 ppm. ¹⁰⁹Ag NMR (27.9 MHz, CDCl₃): 1116.7 (d, J_{AgH} = 41.1 Hz). UV–vis [λ_{max} in nm, (ε in M⁻¹ cm⁻¹)], 374 (21,200). ESI-MS (m/z) [M+Ag]⁺ (Cal.): 1974.07 (1974.16). IR, cm⁻¹: 2980.6(m), 961.8(s), 770.3(m), 637.9(s), 521.5(m).**

[Ag₇(D){S₂P(OEt)₂}]₆, **4_D. It can be obtained via a similar procedure as for **4_H**, using NaBD₄ instead of NaBH₄. Yield: 0.202 g (69%). Mp: 134 °C (dec). Anal. calcd for C₂₄H₆₀DAg₇O₁₂P₆S₁₂: C, 15.43; H, 3.34. Found: C, 15.71; H, 3.33%. ¹H NMR (300 MHz, CDCl₃): 1.34 (t, ³J_{HH} = 6.9 Hz, 36H, CH₃), 4.15 (m, 24H, CH₂), ²H NMR (46.1 MHz, CHCl₃): 6.33 (bs, 1D, 298 K), ³¹P NMR (121.49 MHz, CDCl₃): 111.8 ppm.**

Formation of Silver Nanoparticles. [Ag₇(H){S₂P(OEt)₂}]₆ (0.413 g, 0.221 mmol) and borohydride (0.067 g, 1.763 mmol) in 20 mL of methanol was stirred at room temperature for 1 h under nitrogen. The solution was centrifuged for 30 min, then filtered to get precipitates. They were dried under vacuum to obtain silver nanoparticles. Yield: 0.201 g (98%).

X-ray Crystallography. Crystals were mounted on the tip of glass fibers with epoxy resin. Data were collected on a Bruker APEXII CCD diffractometer using graphite monochromated Mo Kα radiation (λ = 0.71073 Å). Data reduction was performed with XSCANS²¹ and/or SAINT,²² which corrects for Lorentz and polarization effects. An empirical absorption correction based on SADABS²³ was performed. Structures were solved by the use of direct methods, and refinement was

performed by the least-squares methods on F^2 with the SHELXL-97 package,²⁴ incorporated in SHELXTL/PC V5.10.²⁵ Crystal data for 3: $C_{36}H_{85}Ag_7O_{12}P_6Se_{12}$: $T = 296$ K, trigonal, space group $R(-)3$, $a = 22.681(2)$, $c = 12.777(1)$ Å, $V = 5692.4(9)$ Å³, $Z = 3$, $\rho_{\text{calcd}} = 2.274$ g cm⁻³, $\mu = 7.692$ mm⁻¹, $2\theta_{\text{max}} = 56.68^\circ$, $R1 = 0.0456$ [$I > 2\sigma(I)$], $wR2 = 0.1296$ for 2185 data (3151 independent), and 116 parameters. Max./min. $2.233/-0.594$ e/Å³. Crystal data for 4: $C_{24}H_{61}Ag_7O_{12}P_6S_{12}$: $T = 253$ K, trigonal, space group $R(-)3$, $a = 21.087(3)$, $c = 11.6295(16)$ Å, $V = 4478.6(11)$ Å³, $Z = 3$, $\rho_{\text{calcd}} = 2.077$ g cm⁻³, $\mu = 2.872$ mm⁻¹, $2\theta_{\text{max}} = 50.22^\circ$, $R1 = 0.0605$ [$I > 2\sigma(I)$], $wR2 = 0.1733$ for 1221 data (1764 independent), and 129 parameters. Max./min. $0.811/-0.937$ e/Å³.

Computational Details. Geometry optimizations at the density functional theory (DFT) level were carried out on the models $Ag_7(H)(Se_2PH_2)_6$ (3') and $Ag_7(H)(S_2PH_2)_6$ (4') using the Gaussian 09 package,²⁶ employing the BP86 functional,²⁷ and using the general triple- ζ polarized basis set, namely, the Def2-TZVPP set from EMSL Basis Set Exchange Library,²⁸ with an all-electron basis set on silver. The optimized geometries, fully characterized as true minima via analytical frequency calculations, were found to be of C_3 symmetry. The geometries obtained from DFT calculations were used to perform natural orbital population analysis by the NBO 5.0 program.²⁹ The compositions of the molecular orbitals were calculated using the AOMix program.³⁰

The gauge including atomic orbital (GIAO)³¹ method has been used to compute the ¹H chemical shifts, $\delta = \sigma^{\text{TMS}} - \sigma^{\text{cluster}}$, where σ^{TMS} and σ^{cluster} are, respectively, the isotropic chemical shielding of ¹H in tetramethylsilane and in the $[Ag_7(H)(E_2PH_2)_6]^+$ ($E = Se, S$) cluster.

The UV–visible transitions were calculated by means of time-dependent DFT (TDDFT) calculations,³² using the same BP86 functional, but with a smaller basis set, namely, the general double- ζ polarized LANL2DZ basis set^{33a–d} augmented with Ahlrichs polarization functions on all atoms,^{33e} to reduce the computational demand. It has been checked before on test calculations that this basis set change does not modify significantly the energy of the first low energy transitions. Only singlet–singlet, that is, spin-allowed, transitions have been computed. The simulated UV–visible spectra (Supporting Information, Figure S3) were obtained from the computed TDDFT transitions and their oscillator strengths by using the SWizard program,³⁴ each transition being associated with a Gaussian function of half-height width equal to 1500 cm⁻¹.

■ ASSOCIATED CONTENT

Supporting Information

Cartesian coordinates of the optimized structures, simulated UV–vis absorption spectra, and TGA. CCDC 886251 (3), 886252 (4). This material is available free of charge via the Internet at <http://pubs.acs.org>.

■ AUTHOR INFORMATION

Corresponding Author

*E-mail: chenwei@mail.ndhu.edu.tw (C.W.L.), jean-yves.saillard@univ-rennes1.fr (J.-Y.S.). Phone: +886-3-8633607 (C.W.L.). Fax: +886-3-8633570 (C.W.L.).

Notes

The authors declare no competing financial interest.

■ ACKNOWLEDGMENTS

Financial support from the National Science Council of Taiwan (NSC 100-2113-M-259-003-MY3) and the Institut Universitaire de France are gratefully acknowledged.

■ REFERENCES

(1) (a) Daniel, M. C.; Astruc, D. *Chem. Rev.* **2004**, *104*, 293–346. (b) Schmid, G. *Chem. Soc. Rev.* **2008**, *37*, 1909–1930. (c) Diez, I.; Ras, R. H. A. *Nanoscale* **2011**, *3*, 1963–1970. (d) Noble metal nanoparticles, Sreepasad, T. S.; Pradeep, T. *Springer Handbook on Nanomaterials*; Springer: Berlin, Germany, 2012.

(2) Jadzinsky, P. D.; Calero, G.; Ackerson, C. J.; Bushnell, D. A.; Kornberg, R. D. *Science* **2007**, *318*, 430–433.

(3) Heaven, M. W.; Dass, A.; White, P. S.; Holt, K. M.; Murray, R. W. *J. Am. Chem. Soc.* **2008**, *130*, 3754–3755.

(4) Zhu, M.; Eckenhoff, W. T.; Zhu, Y.; Pintaur, T.; Jin, R. *J. Phys. Chem. C* **2008**, *112*, 14221.

(5) Qian, H.; Eckenhoff, W. T.; Zhu, Y.; Pintaur, T.; Jin, R. *J. Am. Chem. Soc.* **2010**, *132*, 8280–8281.

(6) (a) Brust, M.; Fink, J.; Bethell, D.; Schiffrin, D. J.; Kiely, C. J. *Chem. Soc., Chem. Commun.* **1995**, 1655–1656. (b) Parker, J. F.; Fields-Zinna, C. A.; Murry, R. W. *Acc. Chem. Res.* **2010**, *43*, 1289–1296.

(7) Gold-only hydride complexes were reported in four cases: two are stabilized by a carbene,^{a, b} one by a xantphos-phosphole ligand,^c and the other is Au(III) chelated by a rigid (C^NN^C) pincer.^d (a) Tsui, E. Y.; Muller, P.; Sadighi, J. P. *Angew. Chem., Int. Ed.* **2008**, *47*, 8937–8940. (b) Gaillard, S.; Slawin, A. M. Z.; Nolan, S. P. *Chem. Commun.* **2010**, *46*, 2742–2744. (c) Escalle, A.; Mora, G.; Gagosz, F.; Mezailles, N.; Le Goff, X. F.; Jean, Y.; Le Floch, P. *Inorg. Chem.* **2009**, *48*, 8415–8422. (d) Rosca, D.-A.; Smith, D. A.; Hughes, D. L.; Bochmann, M. *Angew. Chem., Int. Ed.* **2012**, *51*, 10643–10646.

(8) Liao, P.-K.; Liu, K.-G.; Fang, C.-S.; Liu, C. W.; Fackler, J. P., Jr.; Wu, Y.-Y. *Inorg. Chem.* **2011**, *50*, 8410–8417.

(9) (a) Liu, C. W.; Chang, H.-W.; Sarkar, B.; Saillard, J.-Y.; Kahlal, S.; Wu, Y.-Y. *Inorg. Chem.* **2010**, *49*, 468–475. (b) Liu, C. W.; Chang, H.-W.; Fang, C.-S.; Sarkar, B.; Wang, J.-C. *Chem. Commun.* **2010**, *46*, 4571–4573.

(10) Liu, C. W.; Liaw, P.-K.; Feng, C.-S.; Saillard, J.-Y.; Kahlal, S.; Wang, J.-C. *Chem. Commun.* **2011**, *47*, 5831–5833.

(11) Wu, Z.; Lanni, E.; Chen, W.; Bier, M. E.; Ly, D.; Jin, R. *J. Am. Chem. Soc.* **2009**, *131*, 16672–16674.

(12) Rao, T. U. B.; Nataraju, B.; Pradeep, T. *J. Am. Chem. Soc.* **2010**, *132*, 16304–16307.

(13) (a) Xiang, H.; Wei, S.-H.; Gong, X. *J. Am. Chem. Soc.* **2010**, *132*, 7355–7360. (b) Balasubramanian, Y. S. K.; Rao, T. U. B.; Pradeep, T. *J. Phys. Chem. C* **2011**, *115*, 20380–20387.

(14) (a) Liu, C. W.; Shang, I.-J.; Hung, C.-M.; Wang, J.-C.; Keng, T.-C. *Dalton Trans.* **2002**, 1974–1979. (b) Zhu, Y. B.; Lu, S. F.; Huang, X. Y.; Huang, Z. X.; Wu, Q. *J. Chin. J. Chem.* **2005**, 2300.

(15) Wang, C.; Haushalter, R. C. *Inorg. Chim. Acta* **1999**, *288*, 1–6.

(16) Casanova, D.; Llundell, M.; Alemany, P.; Alvarez, S. *Chem.—Eur. J.* **2005**, *11*, 1479–1494.

(17) Liao, P.-K.; Fang, C.-S.; Kahlal, A. J. S.; Saillard, J.-Y.; Liu, C. W. *Inorg. Chem.* **2012**, *51*, 6577–6591.

(18) Xie, F.; Baker, M. S.; Goldys, E. M. *J. Phys. Chem. B* **2006**, *110*, 23085–23091.

(19) Jin, R.; Cao, Y. W.; Mirkin, C. A.; Kelly, K. L.; Schatz, G. C.; Zheng, J. G. *Science* **2001**, *294*, 1901–1903.

(20) Sarker, B.; Fang, C.-S.; You, L.-Y.; Wang, J.-C.; Liu, C. W. *New J. Chem.* **2009**, *33*, 626–633.

(21) XSCANS, Release 2.21; Siemens Energy and Automation, Inc.: Madison, WI, 1995.

(22) SAINT, Software for the CCD Detector System, V4.043; Bruker Analytical X-ray System: Madison, WI, 1995.

(23) Sheldrick, G. M. SADABS; University of Göttingen: Göttingen, Germany, 1996.

(24) Sheldrick, G. M. SHELXL-97, Program for the Refinement of Crystal Structure; University of Göttingen: Göttingen, Germany, 1997.

(25) SHELXL 5.10 (PC version) Program Library for Structure Solution and Molecular Graphics; Bruker Analytical X-ray System: Madison, WI, 1998.

(26) Frisch, M. J.; Trucks, G. W.; Schlegel, H. B.; Scuseria, G. E.; Robb, M. A.; Cheeseman, J. R.; Scalmani, G.; Barone, V.; Mennucci, B.; Petersson, G. A.; Nakatsuji, H.; Caricato, M.; Li, X.; Hratchian, H. P.; Izmaylov, A. F.; Bloino, J.; Zheng, G.; Sonnenberg, J. L.; Hada, M.; Ehara, M.; Toyota, K.; Fukuda, R.; Hasegawa, J.; Ishida, M.; Nakajima, T.; Honda, Y.; Kitao, O.; Nakai, H.; Vreven, T.; Montgomery, J. A., Jr.; Peralta, J. E.; Ogliaro, F.; Bearpark, M.; Heyd, J. J.; Brothers, E.; Kudin, K. N.; Staroverov, V. N.; Kobayashi, R.; Normand, J.; Raghavachari, K.; Rendell, A.; Burant, J. C.; Iyengar, S. S.; Tomasi, J.; Cossi, M.; Rega, N.;

Millam, J. M.; Klene, M.; Knox, J. E.; Cross, J. B.; Bakken, V.; Adamo, C.; Jaramillo, J.; Gomperts, R.; Stratmann, R. E.; Yazyev, O.; Austin, A. J.; Cammi, R.; Pomelli, C.; Ochterski, J. W.; Martin, R. L.; Morokuma, K.; Zakrzewski, V. G.; Voth, G. A.; Salvador, P.; Dannenberg, J. J.; Dapprich, S.; Daniels, A. D.; Ö. Farkas, Foresman, J. B.; Ortiz, J. V.; Cioslowski, J.; Fox, D. J. *Gaussian 09*, Revision A.1; Gaussian, Inc.: Wallingford, CT, 2009.

(27) (a) Becke, A. D. *Phys. Rev. A* **1988**, *38*, 3098–30100. (b) Perdew, J. P. *Phys. Rev. B* **1986**, *33*, 8822–8824.

(28) Weigend, F.; Ahlrichs, R. *Phys. Chem. Chem. Phys.* **2005**, *7*, 3297–3305.

(29) Glendening, E. D.; Badenhoop, J. K.; Reed, A. E.; Carpenter, J. E.; Bohmann, J. A.; Morales, C. M.; Weinhold, F. *NBO 5.0*; Theoretical Chemistry Institute, University of Wisconsin: Madison, WI, 2001; <http://www.chem.wisc.edu/~nbo5>.

(30) Gorelsky, S. I. *AOMix program*; <http://www.sg-chem.net/>

(31) (a) London, F. J. *Phys. Radium* **1937**, *8*, 397–409. (b) McWeeny, R. *Phys. Rev.* **1962**, *126*, 1028–1034. (c) Ditchfield, R. *Mol. Phys.* **1974**, *27*, 789–807. (d) Dodds, J. L.; McWeeny, R.; Sadlej, A. J. *Mol. Phys.* **1977**, *34*, 1779–1791. (e) Wolinski, K.; Hinton, J. F.; Pulay, P. *J. Am. Chem. Soc.* **1990**, *112*, 8251–8260.

(32) Burke, K.; Gross, E. K. U. A guided tour of Time-Dependent Density Functional Theory. In *Density Functionals: Theory and Applications*; Joubert, D., Ed.; Springer: Berlin, Germany, 1998; Vol. 500.

(33) (a) Dunning, Jr. T. H.; Hay, P. J. *Methods of Electronic Structure Theory*; Schaeffer, H. F., Ed.; Plenum Press: New York, 1977. (b) Hay, P. J.; Wadt, W. R. *J. Chem. Phys.* **1985**, *82*, 270–283. (c) Hay, P. J.; Wadt, W. R. *J. Chem. Phys.* **1985**, *82*, 284–298. (d) Hay, P. J.; Wadt, W. R. *J. Chem. Phys.* **1985**, *82*, 299–310. (e) Schafer, A.; Horn, H.; Ahlrichs, R. *J. Chem. Phys.* **1992**, *97*, 2571–2577.

(34) Gorelsky, S. I. *SWizard program*, revision 4.5; <http://www.sg-chem.net/>.